Blockade of ActRIIB signaling triggers muscle fatigability and metabolic myopathy

Blockade of ActRIIB signaling triggers muscle fatigability and metabolic myopathy

Karima Relizani[1,2,3], Etienne Mouisel[1,4], Benoit Giannesini[5], Christophe Hourdé[1], Ketan Patel[6], Susanne Morales Gonzales[2], Kristina Jülich[1,2], Alban Vignaud[1,7], France Piétri-Rouxel[1], Dominique Fortin[8], Luis Garcia[3], Stéphane Blot[9], Olli Ritvos[10], David Bendahan[5], Arnaud Ferry[1,11], Renée Ventura-Clapier[8], Markus Schuelke[2] and Helge Amthor[1,3,12]

[1]Université Pierre et Marie Curie, Institut de Myologie, Unité mixte de recherche UPMC-AIM UM 76, INSERM U 974, CNRS UMR 7215, 75013 Paris, France; [2]Department of Neuropediatrics & NeuroCure Clinical Research Center, Charité Universitätsmedizin Berlin, 13353 Berlin, Germany; [3]UFR des Sciences de la Santé, Université de Versailles Saint-Quentin-en-Yvelines, 78180 Montigny-le-Bretonneux, France;[4]Inserm UMR 1048, Université Paul Sabatier, Toulouse, France (present address); [5]Aix-Marseille Université, Centre National de la Recherche Scientifique (CNRS), Centre de Resonance Magnetique Biologique et Medicale UMR 7339, 13385, Marseille, France; [6]School of Biological Sciences, University of Reading, Reading, UK; [7]Généthon, 1 bis rue de l'Internationale, 91002 Evry, France; [8]INSERM U 769, Université Paris-Sud, Châtenay-Malabry, France; [9]Unité de Neurologie, Ecole Nationale Vétérinaire d'Alfort, Université Paris Est, France; [10]Department of Bacteriology and Immunology, Haartman Institute, University of Helsinki, Helsinki, Finland; [11]Université Paris Descartes, 75006 Paris, France; [12]Service Génétique Médicale, CHU Necker-Enfants Malades, Université Paris Descartes, France.

Correspondence should be addressed to:

Helge Amthor, MD, PhD
Laboratoire «Biothérapies des Maladies du Système Neuromusculaire»
UFR des Sciences de la Santé «Simone Veil»
Université de Versailles Saint-Quentin-en-Yvelines
2, avenue de la Source de la Bièvre
78180 Montigny-le-Bretonneux, France
Email: helge.amthor@uvsq.fr

or

Markus Schuelke, MD
NeuroCure Clinical Research Center and Department of Neuropediatrics
Charité Universitätsmedizin Berlin
Augustenburger Platz 1
D-13353 Berlin, Germany
Email: markus.schuelke@charite.de

Short title: ActRIIB blockade triggers metabolic myopathy

Abstract

Myostatin regulates skeletal muscle size *via* the activin receptor IIB (ActRIIB). However, its effect on muscle energy metabolism and energy dependent muscle function remains largely unexplored. This question needs to be solved urgently since various therapies for neuromuscular diseases based on blockade of ActRIIB signaling are being developed. Here we show in mice that four months of pharmacological abrogation of ActRIIB signaling by treatment with soluble ActRIIB-Fc triggers extreme muscle fatigability. This is associated with elevated serum lactate levels and a severe metabolic myopathy in the *mdx* mouse, an animal model of Duchenne muscular dystrophy. Blockade of ActRIIB signaling down-regulates Porin, a crucial ADP/ATP shuttle between cytosol and mitochondrial matrix leading to a consecutive deficiency of oxidative phosphorylation as measured by *in vivo* Phophorus Magnetic Resonance Spectroscopy (^{31}P-MRS). Further, ActRIIB blockade reduces muscle capillarization, which further compounds the metabolic stress. We show that ActRIIB regulates key determinants of muscle metabolism, such as Pparβ, Pgc1α, and Pdk4 thereby optimizing different components of muscle energy metabolism. In conclusion, ActRIIB signaling endows skeletal muscle with high oxidative capacity and low fatigability. The severe metabolic side effects following ActRIIB blockade caution against deploying this strategy, at least in isolation, for treatment of neuromuscular disorders.

Key words: ActRIIB, myostatin, metabolic myopathy, muscle fatigue, oxidative phosphorylation, beta-oxidation, Duchenne muscular dystrophy, mdx mouse.

INTRODUCTION

Skeletal muscle has inbuilt control mechanisms to prevent overgrowth. This function is executed, at least in part, by secreted molecules including members of the transforming growth factor-β (TGF-β) family, especially myostatin[1]. Myostatin signals *via* its transmembrane activin receptor IIB (ActRIIB) and suppression of this pathway stimulates muscle growth[2,3]. In the past few years, strategies have been developed to treat muscular dystrophies, muscle wasting and cachexia by blocking the myostatin/ActRIIB pathway with first of many clinical trials already being concluded (ClinicalTrials.gov NCT01099761, NCT01519349, NCT01423110, NCT01669174, NCT01601600, NCT01433263). However, it remains a matter of controversy whether the hypertrophic muscles that form as a result of blocking myostatin/ActRIIB signaling confer any functional benefit, because a number of groups have reported loss of specific force of larger muscles in myostatin knockout mice and a faster fatigability ($Mstn^{-/-}$)[4-6]. In addition, myostatin knockout leads to a change of muscle contractile and metabolic characteristics towards a "glycolytic" phenotype[5,7,8], commonly attributed to a change in muscle specification during development. In contrast to the constitutive myostatin deficiency of $Mstn^{-/-}$ mice, postnatal treatment with soluble activin IIB receptor (sActRIIB-Fc) in adult mice blocks myostatin/ActRIIB signaling and increases muscle force without altering the fiber type composition[9,10]. Similar results have been obtained in the *mdx* mouse model of Duchenne muscular dystrophy[11,12]. However, a recent transcriptome profiling demonstrated a down-regulation of genes involved in oxidative phosphorylation and mitochondrial function following treatment with sActRIIB-Fc.[13] Another study revealed a faster decline of muscle force following repetitive stimulation[14]. Whether those changes reflect solely a change towards a faster muscle phenotype or a relevant mitochondrial dysfunction is presently unknown. In the view of ongoing clinical trials we need to address the question of how myostatin blockade affects the metabolism of dystrophic muscle in *mdx* mice, which already has a preexisting deficit of mitochondrial function[15-17]. Here we explored the hypothesis that ActRIIB signaling is a key regulator of oxidative metabolism in the adult muscle. We thus set out to systematically investigate in adult wild-type and *mdx* mice, how postnatal blockade of ActRIIB signaling using sActRIIB-Fc might affect muscle energy metabolism and energy dependent muscle function. Our data conclusively show the importance of ActRIIB signaling as a pivotal link that acts to balance muscle size and strength against endurance capacity *via* optimization of energy metabolism.

RESULTS

ActRIIB blockade in adult wild-type mice increases fatigability. Muscles of *Mstn*$^{-/-}$ mice, a model of constitutive inhibition of signaling *via* ActRIIB, exhibit a congenital fiber-type profile that is characterized by an increase in the number of fast "glycolytic" (MHCIIB) fibers and concomitant loss of "oxidative" (MHCI, MHCIIA) fibers, which entails changes in muscle function, exercise capacity and muscle metabolism[4,7,8,18,19]. To circumvent the effects of congenital fiber-type switching, we here inhibited ActRIIB signaling in adult wild-type mice with a soluble form of the activin receptor fused with the Fc-fragment of mouse IgG (sActRIIB-Fc). Four months of treatment promoted robust skeletal muscle growth together with a significant increase in total body weight, confirming previously published data (**Fig. S1**)[20]. Importantly, the increase in muscle mass was not accompanied by fiber-type conversion (**Fig. S2**). The absolute maximal force of *EDL* and *soleus* muscle increased in parallel with muscle size (**Figs. 1a,c**). Specific maximal force was conserved, implicating a proportional increase of force and muscle mass (**Fig. 1b**). However, sActRIIB-Fc treatment also increased muscle fatigue (**Figs. 1c,d**) and mice exhausted precociously during incremental speed running tests (**Figs. 1e,g**). Serum lactate, being already significantly increased at resting state, rose to pathological levels following incremental speed running (**Figs. 1f,g**). The concept of "Critical Speed" accurately reflects the capacity for aerobic exercise and is based on the proportional relationship between "covered distance" and "time to exhaustion" at different velocities[21]. During the four months treatment period, we found a steady decline in Critical Speed in the treatment and control group, however, the decline over time was by far larger in sActRIIB-Fc treated animals as compared to PBS-treated mice (**Figs. 1h,i**).

Severe exercise intolerance in dystrophic mdx mice following treatment with sActRIIB-Fc. In Duchenne muscular dystrophy and its *mdx* mouse model, oxidative metabolism is compromised due to membrane damage and the resulting intracellular calcium overload[15-17]. Having shown that ActRIIB blockade decreased aerobic exercise capacity in wild-type mice, we now investigated what effect administration of sActRIIB-Fc would have on the metabolic phenotype of *mdx* mice. This information would have important clinical implications for the strategies to use ActRIIB blockade for treatment of muscular dystrophies. Despite a massive increase in skeletal muscle mass after sActRIIB-Fc treatment (**Fig. S1**), absolute maximal force decreased in *soleus* muscle and most notably specific force in both *EDL* and *soleus* muscles (**Figs. 2a,b**), serving as functional evidence for increased myopathic changes of sActRIIB-treated dystrophic *mdx* muscle. Interestingly, sActRIIB-Fc treatment did not cause any

greater force decline during repetitive stimulation (**Figs. 2c,d**). Electromyography excluded problems in neuromuscular transmission but revealed abnormal spontaneous potentials and the presence of complex repetitive discharges in both PBS and sActRIIB-Fc treatment groups of the *mdx* mice **(Fig. S3)**. Such polyphasic potentials are characteristic of dystrophic *mdx* muscle[22]. As voluntary motor activity seemed reduced when observing sActRIIB-Fc treated *mdx* mice, we proceeded to analyze their exercise behavior. Remarkably, at the end of the treatment period, sActRIIB-Fc treated *mdx* mice suffered from severe exercise intolerance associated with a pathological serum lactate increase (**Figs. 2e-g, Supplemental Video**). It is important to note, that exercise capacity of *mdx* mice declined throughout the four months treatment period, however, to a far larger extent in sActRIIB-Fc treated *mdx* mice than in the PBS-treated control group (**Figs. 2h,i**).

sActRIIB-Fc treatment affects muscle capillarization. The ability of mitochondria to produce ATP critically depends on the oxygen supply *via* tissue blood perfusion, thus a combination of hypoperfusion plus exercise induced hypoxemia might explain the severe exercise intolerance. Treatment with sActRIIB-Fc caused a drop in capillary density especially in the oxidative *soleus* muscle from *mdx* mice with a subsequent increase in the capillary domain (**Figs. 3a-d**). The increase of the capillary domain was also found in glycolytic *EDL* muscles of *mdx* mice, albeit to a lesser degree (**Fig. S4a-d**). Treatment of mice as well as of C_2C_{12} myotubes with sActRIIB-Fc down-regulated expression of *Vegf-A* suggesting an indirect negative effect of myostatin blockade on capillary formation (**Figs. 3e,f**). Interestingly, *Vegf-A* expression in *mdx* mice was much lower than in wild-type mice, and treatment with sActRIIB-Fc did not decrease *Vegf-A* mRNA-abundance any further (**Fig. 3e**), suggesting the presence of additional mechanisms for regulating capillary density. In this regard the findings of Hayot *et al.* (2010) are of special interest, who reported an induction of myostatin expression in muscles of rats exposed to chronic hypoxia and in patients with chronic obstructive pulmonary disease (COPD). The authors interpreted these findings as a potential cause for the muscle wasting that is often seen in COPD-patients[23]. These findings, however, could also be interpreted as a compensatory up-regulation of myostatin to improve the metabolic functioning and to increase capillary density in a state of chronic hypoxia. It is of special interest that endothelial cells strongly express the mRNAs of transmembrane receptors (*ActRIIA/B* and ALK4/5) for myostatin or its homologs, whereas *myostatin* mRNA was only expressed at low levels (**Fig. 3g**). Treatment of endothelial cells (HUVEC cell line) with increasing dosages of recombinant myostatin *in vitro* increased the cell doubling time in culture, verifying a direct

effect of myostatin or its homologs on endothelial cell proliferation (**Fig. S4e**), however, the exact ligands of muscle endothelial cell regulation *in vivo* remain to be determined.

ActRIIB signaling regulates Pgc1α and Ppar transcription factors. The exercise intolerance and lactic acidosis following ActRIIB blockade suggests underlying changes in muscle metabolism, a hypothesis supported by previous transcriptome profiling[13]. In agreement, we show that the copy numbers of *Pgc1α* and *Pparβ,* which are key transcription factors promoting oxidative metabolism in skeletal muscle, are down-regulated after treatment with sActRIIB-Fc (**Figs. 4b,c**) and following treatment of C_2C_{12} myotubes with sActRIIB-Fc (**Fig. 4g**). On the protein level, down-regulation of Pgc1α was more pronounced in the *mdx* muscle if referred to desmin abundance (**Fig. 4a**). Such loss of oxidative properties was accompanied by a compensatory activity increase of enolase, a key glycolytic enzyme (**Fig. 4d**). Furthermore, mRNA levels of *Pdk4*, an inhibitor of pyruvate dehydrogenase (Pdh) and a regulatory switch of substrate utilization from glucose towards fatty acids[24], was strongly decreased following sActRIIB-Fc treatment in *mdx* mice (**Fig. 4e**). We thus expected an inhibitory effect of sAcvRIIB-Fc treatment on β-oxidation and found a down-regulation of *Cpt1b* mRNA levels (**Fig. 4f**). Likewise, sActRIIB-Fc treatment of C_2C_{12} myotubes reduced expression of genes controlling oxidative metabolism and β-oxidation within 24 hours of treatment (**Fig. 4g**), implying a direct effect of myostatin signaling in the regulation of these genes.

We further focused our attention on the neuronal nitric oxide synthase (Nos1, nNos), because it is well known that the sarcolemmal presence of the Nos1 enzyme is strongly reduced in the absence of its binding partner dystrophin in patients with DMD and in *mdx* mice[25,26]. The resulting dysregulation of NO-synthesis entails a failure of contraction induced vasodilatation as well as changes in the cellular calcium homeostasis associated with exacerbated post-exercise fatigability, exercise-induced muscle edema and cell necrosis[27,28]. We thus wondered, whether sActRIIB-Fc treatment would influence sarcolemmal Nos1 expression, hence further compromising the pathophysiological effect of sActRIIB-Fc on vasculature and oxidative metabolism. As expected, we found a strong decrease of *Nos1* mRNA copy numbers in *mdx* muscles of both treatment groups in comparison to wild-type muscle (**Fig. S11a**), which was paralleled by a strong decrease of sarcolemmal expression of Nos1 protein in *mdx* muscle (**Fig. S11b**). Furthermore, treatment with sActRIIB-Fc diminished *Nos1* transcription in wild-type and *mdx* muscle (**Fig. S11a**). However, subsarcolemmal Nos1 protein content remained unchanged (**Fig. S11b**), and Western blot did not reveal any changes in Nos1 protein levels in wild-type mice (**Fig. S11c**), whereas Nos1 protein levels in *mdx* mice were below detection

levels (data not shown). This suggests that sActRIIB-Fc treatment unlikely aggravates NO dysregulation of dystrophin deficient muscle, although further experiments are required to ascertain or to exclude a role of the ActRIIB-receptor on NO signaling.

Reduced oxidative metabolism in mdx muscle following treatment with sActRIIB-Fc. It should be noted that the mRNA and protein levels of key regulatory genes (Pparβ, Pgc1α) important for oxidative metabolism (**Figs. 4a-c**) were significantly lower in *mdx* than in wild-type mice, supporting previous findings that oxidative muscle metabolism is depressed in dystrophic muscle to some extent[15,29].

We therefore studied in real-time the response of the oxidative metabolism to a standardized bout of exercise in anesthetized *mdx* mice either treated with PBS (controls) or sActRIIB-Fc. Muscle function and energy metabolism were assessed strictly noninvasively in calf muscle with an innovative experimental setup using phosphorus (^{31}P) nuclear magnetic resonance spectroscopy (MRS)[30]. An exercise bout of six minutes consisting of repeated maximal isometric contractions was induced *in vivo* by transcutaneous electro-stimulation. After induced repeated contractions fatigue levels (**Fig. 5a**), intracellular acidosis (**Fig. 5b**) as well as phosophocreatine (PCr) consumption (**Fig. 5c**) were similar in both groups. However, the time constant of post-exercise phosphocreatine re-synthesis (τPCr) was significantly prolonged in sActRIIB-Fc treated *mdx* mice **(Figs. 5d,e)**. Given that PCr synthesis during the post-exercise recovery period relies exclusively on oxidative ATP synthesis, τPCr has largely been acknowledged as an important *in vivo* index of oxidative mitochondrial capacity. Hence the prolonged τPCr demonstrates that sActRIIB-Fc treatment reduces oxidative metabolism *in vivo*.

The MRS results pointed to an underlying functional deficit of the skeletal muscle respiratory chain complexes or β-oxidation in response to sActRIIB-Fc treatment. However, contrary to our hypothesis, we found **(i)** largely unaffected *ex vivo* activities of isolated key mitochondrial enzymes (Krebs cycle: citrate synthase [CS]; respiratory chain: cytochrome C oxidase [COX]; and β-oxidation: hydroxyacyl-CoA-dehydrogenase [HADHA]) and **(ii)** similar succinate dehydrogenase [SDH] and COX fiber profiles (**Figs. S5-S7**). In fact, COX and SDH enzyme activities even appeared somewhat increased in *EDL* muscles (**Figs. S5c,d, S6a, S7a**), likely reflecting a compensatory increase in response to decreased aerobic energy production. Furthermore, mitochondrial DNA (mtDNA) copy numbers remained largely unchanged following treatment with sActRIIB-Fc (**Fig. S8a**). The normal mtDNA copy numbers together with unaltered CS enzyme activities (**Fig. S5a,b**) let us conclude that ActRIIB blockade did not affect mitochondrial mass.

Treatment with sActRIIB-Fc down-regulates porin expression in wild-type and mdx muscle. Given the abnormal post-exercise PCr re-synthesis (τPCr) along with normal respiratory chain activities, we wondered whether the ATP transport from the mitochondrial matrix into the cytosol of skeletal muscle cells might be affected, which might explain the diminished rate of aerobic energy production. Keeping with such hypothesis, decreased protein levels of Vdac3 had already been reported for *mdx* muscle, hinting towards a derangement of the ADP/ATP-shuttling system through the outer mitochondrial membrane *via* the Voltage Dependent Anion Channels (Vdac, syn. porin)[31,32,33]. In line with these findings, a proteomic survey of differentially expressed proteins from wild-type and *mdx* mouse hearts had discovered a substantial loss of Vdac1 protein[34]. Indeed, here we show that wild-type and to an even larger extent *mdx* muscles exhibited a considerable reduction of *Porin* mRNA-transcripts (**Fig. S8a**) and porin protein levels (**Fig. S9**) after sActRIIB-Fc treatment. This pushes the muscle even further into global mitochondrial dysfunction than dystrophin deficiency alone. Such secondary mitochondriopathy might explain the high lactic acidosis and rapid fatigability of sActRIIB-Fc treated *mdx* mice.

Myopathic changes in mdx mice following treatment with sActRIIB-Fc. We next investigated the consequences of sActRIIB-Fc treatment on the extent of muscle dystrophy in *mdx* mice. Muscles from both sActRIIB-Fc and PBS-treatment groups revealed typical dystrophic changes comprising muscle fiber necrosis, regenerating fibers, fibers with central nuclei, inflammatory infiltrates, and increased fibrosis, which are difficult to quantify (**Fig. S10a**). Muscle degeneration is accompanied by a leak of cytoplasmic enzymes such as creatine kinase (CK). We measured serum CK levels, which were largely elevated in *mdx* mice from both treatment groups; however, we did not detect any significant differences since inter-individual variation was large (**Fig. S10b**). In *mdx* mice, muscle degeneration is followed by excessive regeneration with abundant splitting of regenerated fibers, which appear as small fiber profiles on transverse sections. Such excessive regeneration leads to an increase of muscle mass (see comparison between wild-type and *mdx* mice: **Fig. S1**). Following treatment with sActRIIB-Fc, muscles enlarged on average, if compared to PBS treatment, by ≈1.6 fold in *mdx* and by ≈1.3 fold in wild-type mice (**Fig. S1**). However, analysis of morphometric features of *EDL* muscles from sActRIIB-Fc treated *mdx* mice, revealed a further increase in the number of small fiber profiles if compared to PBS-treated *mdx* mice (**Fig. S10c**). This finding suggestes that the excessive increase of muscle weight was triggered by abnormal regeneration and not by fiber hypertrophy. The *soleus* muscle of *mdx* mice, while not increasing its

mass after sActRIIB-Fc treatment, exhibited an increased fiber size variation (**Fig. S10d**). In conclusion, the dystrophic phenotype of dystrophin deficient muscle persisted or even increased following treatment with sActRIIB-Fc.

DISCUSSION

Myostatin/ActRIIB signaling exerts three major functions on skeletal muscle. **(i)** It acts to limit its size, **(ii)** promotes oxidative properties, and **(iii)** balances glucose *versus* fat utilization. The changes in muscle physiology in hypermuscular mice following treatment of adult mice with sActRIIB-Fc highlights the fact that myostatin/ActRIIB blockade confers little functional advantage over wild-type muscle due to its rapid fatigability. Improved muscle strength, however short lived, comes at the cost of increased fatigability and exercise intolerance, which is often seen in patients with mitochondrial disorders such as MELAS or MERRF syndrome[35]. Interestingly, muscle cramps are frequently observed in whippet dogs with homozygous *Mstn* mutations[36]. Moreover, "double muscle cattle", several breeds of which have been identified to carry *Mstn* mutations[37,38], are prone to exercise induced lactic acidosis and severe rhabdomyolysis[39,40]. In myostatin deficient animals, such exercise failure could be attributed to congenital fiber-type disproportion with a shift towards the expression of the fast IIB myosin heavy chain (MHC) isoform[4,18], which is well known to be associated with loss of oxidative properties of skeletal muscle and increased fatigability[5,8]. In contrast to animals born with mutations in the *Mstn* gene, we show that blockade of ActRIIB signaling in adult wild-type mice beyond the period of muscle development does not have any impact on fiber-type composition, thus confirming previous reports[10].

After sActRIIB-Fc treatment, the mice exhibit clinical signs of early muscle fatigue, exercise intolerance, and lactic acidosis – characteristic signs for a depression of β-oxidation, a shift towards anaerobic glycolysis, and ATP-deficiency. Interestingly, whereas *ex vivo* mitochondrial respiratory chain enzyme activities and mtDNA copy numbers were within the normal range, *in vivo* ^{31}P-MRS clearly demonstrated a down-regulation of oxidative energy metabolism in sActRIIB-Fc treated *mdx* mice. We further demonstrate a significant loss of the Porin complex in sActRIIB-Fc treated mice, pointing towards an underlying defect of ATP-handling and ATP-transport as one causative mechanism for the metabolic phenotype. A second aggravating factor, which further compromised exercise tolerance, is the decrease of capillary density and the increase of the capillary domain. Previous reports attributed such reduced capillary density to the increase of muscle fiber size[41]. However, here we demonstrate a net numerical loss of capillaries per fiber following treatment with sActRIIB-Fc. This finding was most pronounced in *mdx* mice with a profound rarefication of the capillary bed in dystrophic muscle. In dystrophinopathies diminished sarcolemmal Nos1 results in dysregulation of the capillary adaptive response to exercise leading to functional muscle ischemia[42].

Our protein analysis argues against a further aggravation of the capillary adaptive response by additional loss of Nos1 in sActRIIB-Fc treated animals, despite the fact that *Nos1* mRNA levels were clearly reduced. sActRIIB-Fc treatment of dystrophic *mdx* mice dramatically worsened the myopathic phenotype as shown by the large deficit in specific force. As lack of dystrophin *per se* alters mitochondrial function in DMD patients and *mdx* mice[15,16,29], the blockade of myostatin signaling initiates a vicious cycle resulting in severe secondary metabolic myopathy. We also found an increased fiber size variation after sActRIIB-Fc treatment of *mdx* mice pointing towards increased myopathic changes even at the tissue level.

In the past, several investigators have used different strategies of interfering with the ActRIIB receptor mediated signaling pathway in order to treat *mdx* mice and GRMD dogs. This was done either through injection of sActRIIB-Fc[12,43], AAV-mediated gene transfer[11] or antibodies directed against the ActRIIB receptor[44]. Overall, the conclusions were optimistic about the usefulness of such strategy to treat dystrophinopathies. However, it should be noted that our results and conclusions differ from previously published work in various aspects. We think the reason for that mainly lies in the choice of endpoints to define success or failure of such a treatment. For DMD patients, clinically relevant and quantifiable improvements would comprise better performance in the six-minutes walk[45] and improvement of respiratory function. This implies the ability of the patient's body to maintain a certain workload for a prolonged time period and not just to be able to produce single bouts of maximum short-duration muscle activity as tested by tetanic muscle contractions[11,12] or by the whole body tension method[43]. In most studies, the increase of muscle size was taken as an endpoint[11,44], automatically assuming that big muscles are healthier muscles. This basic assumption is put into question by our results. None of the studies investigated endurance capacity, which evaluates the effect of a treatment on the physiology of the entire body over a longer time period and would thus be a relevant parameter that could translate into improvement of life quality in patients. Several studies, one using the identical sActRIIB-Fc compound[12], reported a small, but significant decline of CK values after ActRIIB blockade[11,12]. We were unable to reproduce this finding, the reason for these differences remaining unresolved.

We show that myostatin controls the metabolic profile of skeletal muscle, and its blockade depresses the main molecular determinants of oxidative metabolism and β-oxidation. Interestingly, genetic inactivation of *Pparβ*, similar to myostatin/ActRIIB blockade, reduced oxidative properties of skeletal muscle[46]. This adds further evidence that myostatin controls the muscle oxidative phenotype *via* peroxisome proliferator-activated receptors (PPAR) and

Pgc1α, the downstream target of Ppar*β*, while the down-regulation of *Pdk4* indicates a shift away from β-oxidation towards glucose metabolism. These qPCR data are strongly corroborated by a recent transcriptome study following treatment with sActRIIB-Fc of wild-type mice[13]. However, we lack direct evidence to ascertain a shift towards higher glucose metabolism, although the down-regulation of *Pdk4* and up-regulation of Enolase can be counted as indirect indicators for such a change. The unfavorable combination of decreased vascularization and metabolic changes after ActRIIB blockade is likely to cause a rapid imbalance between increased cytosolic ATP hydrolysis and insufficient mitochondrial ATP synthesis during exhaustive exercise. The subsequent shift towards anaerobic glycolytic ATP synthesis explains the rapid fatigability and the pathologically increased lactate production[47]. However, the metabolic adaption in response to myostatin may differ in diverse physiological and pathophysiological contexts, e.g. myostatin inhibition was reported to improve motor performance in aged mice[48]. Further work is required to elucidate the metabolic function of myostatin in different disease situations and during ageing.

In conclusion, our results suggest that myostatin/ActRIIB signaling optimizes oxidative metabolism of skeletal muscle leading to lower muscle fatigability and amelioration of endurance capacity. Such fundamental functions of myostatin should be taken into account in the development of therapies based on myostatin/ActRIIB blockade. However, it should be kept in mind that our experimental design does not allow to determine which effects can be ascribed to myostatin blockade alone and which to the inactivation of other TGF-β family members such as bone morphogenetic proteins (BMP), growth and differentiation factors (GDF) and activins that may also be sequestered by the soluble ActRIIB. Further investigations are required to answer the question, such as whether emerging therapies based on PPAR agonists might be able to prevent such adverse effects of ActRIIB blockade on the oxidative metabolism and on exercise tolerance. Furthermore, dose regime studies could answer the question, whether short-term treatment or pulse treatment may circumvent secondary effects of myostatin/ActRIIB blockade on muscle metabolism.

MATERIALS AND METHODS

Animals. Male *mdx* mice (on a C57BL/10ScSn background) were bred in the animal facility of the Medical Faculty of Paris VI and kept according to institutional guidelines. Wild-type male C57BL/6J control mice were purchased from Charles River (France). Two-months-old wild-type and *mdx* mice were injected twice weekly subcutaneously with 10 mg/kg with the rodent form of the soluble activin receptor IIB (sActRIIB-Fc; Acceleron Pharma) for a total of four months before sacrifice. The methods of sActRIIB-Fc synthesis have previously been described[49]. All animal studies have been approved and were carried out under the laboratory and animal facility licenses A75-13-11 and A91-228-107.

Evaluation of the critical speed. Mice were subjected to three or four separate bouts of runs until exhaustion at various treadmill speeds (between 20 and 80 cm/s according to individual motor capacity, one run per day) according to previously published protocols[21]. Critical Speed, an index of the aerobic exercise capacity, was calculated from the slope (a) of the regression line, plotting the distance (y) against the time to exhaustion (x) from the different runs.

Blood lactate assessment during exhaustive exercise. Lactate concentrations were determined in blood samples collected from the tip of the tail using a *Lactate pro LT* device (Arkray Inc, Kyoto, Japan) at rest before exercise (0 min) and 5 min after treadmill running-induced exhaustion. Exhaustion was defined as the time point at which the mice were unable to run anymore and stayed on the grid despite repeated electric stimulation. The running test started at the lowest speed of 5 cm/s to allow a warm-up and then increased by 1 cm/s every 30 seconds until exhaustion. This protocol is illustrated by the **Supplemental Video,** which demonstrates the running test of sActRIIB-Fc treated wild-type (left) and *mdx* mice (right) side by side. The starting speed of 5 cm/s was increased by 1 cm/s every minute until exhaustion of the *mdx* mouse at 19 cm/s after 14 minutes, while the wild-type mouse was still able to run at a speed of 40 cm/s.

Electromyographic examination. Electromyographic examination of the *triceps brachialis*, *tibialis*, *gastrocnemius* and *quadriceps femoris* muscles was performed in mice anesthetized with isoflurane. Standard non-invasive needle electromyography was conducted on a Viking Quest EMG apparatus (Viasys, Nicolet Biomedical, Madison, Wisconsin) using concentric bipolar needle electrodes. Insertional activity and pathological spontaneous activity were recorded.

Measurement of contractile properties. Absolute maximal isometric tetanic force (P0) was measured during tetanic contractions (frequency of 50-100 Hz, train of stimulation of 1,500 ms for *soleus* and 750 ms for *EDL*). Specific maximal isometric force (sP0) was given as the quotient between force and muscle weight. For analysis of fatigue resistance, muscles were stimulated at 75 Hz for 500 ms, every 2 seconds over 3 minutes. See details in the Online Supplementary Material.

Western blot. Protein was extracted from frozen *tibialis anterior* (TA) muscle of wild-type and *mdx* mice and processed as described[50]. Briefly, after homogenization of the muscle in RIPA buffer with a proteinase inhibitor cocktail (Complete®, Roche-Diagnostics) proteins were separated through denaturating SDS-PAGE with the Laemmli system and blotted onto nitrocellulose membranes by the semidry method (Biometra). The blots were probed with anti-porin as primary antibody (VDAC 31HL, AB-2, Calbiochem), anti-PGC1α (Santa-Cruz), anti-Nos1 (Abcam) and corresponding peroxidase-labeled secondary antibodies. The desmin and GAPDH bands were used as loading control for muscle. Bands were visualized by chemi-luminescence. The protein bands were quantified by measuring their integrated density within a rectangle that covered the entire individual band and subtracting the integrated density of an empty rectangle of exactly the same size in the vicinity using the ImageJ software.

Enzyme measurements. Enolase, citrate synthase [CS], cytochrome C oxidase [COX] and hydroxyacyl-CoA-dehydrogenase [HADHA] activities were determined in extracts from fro-zen cryostat sections using a coupled enzyme assay as detailed in the Online Supplementary Material.

Histology and SDS-PAGE. H&E, SDH and COX staining were performed using routine his-tological protocols. The following primary antibodies were used for immunohistochemistry: anti-CD31 (Pharmingen), anti-MHCIIA (SC-71, DSMZ), anti-MHCI (BAD5, DSMZ), anti-Nos1 (Abcam) and anti-laminin (Dako) followed by secondary antibodies with various fluo-rophores (Alexa Fluor®, Invitrogen). See details in the Online Supplementary Material.

Morphometric analysis of capillary number and capillary domains: Cryosections of 12 µm of the EDL and *soleus* muscles of PBS- and sActRIIB-Fc treated animals were stained with anti-laminin to delineate the muscle fibers. Muscle capillaries were stained with anti-CD31. Fluorescent photographs were taken with a 20x objective on a Microscope (Zeiss, AxioImager Z1) and saved as TIFF files. These images were projected on a flatscreen coupled with a graphic tablet, which enabled the manual retracing of the muscle fiber outlines and the counting of capillaries that were found around it. For the EDL, the fibers of the entire muscle

cross section were analyzed, and for the *soleus* muscle, the fibers from 10 representative non-overlapping visual fields. For each muscle fiber we determined the cross sectional plane [μm^2] and counted the number of bordering capillaries. The capillary domain [μm^2] for each fiber was calculated by dividing its cross sectional plane by the number of bordering capillaries.

Cell Culture. C_2C_{12} cells were grown in DMEM (Gibco 41966-029) supplemented with 1% Pen/Strep and 20% FBS (Gibco 10500-064) to semiconfluency at 37°C and 5% CO_2 for 2 days. Thereafter, the medium was replaced by DMEM + 10% horse serum (Gibco 26050-088) to induce fusion into multinucleated myotubes. sActRIIB-Fc was added to a final concentration of 200 ng/ml to the culture medium of the myotubes. After 24 h, the myotubes were harvested by trypsinization, washed and pelleted for RNA extraction. Human umbilical vein endothelial cells (HUVEC) were grown to confluency, trypsinized and pelleted for RNA extraction. The doubling time of the cells was determined using the AlamarBlue reagents from Invitrogen (UK). Briefly, cells were plated at 20% confluency and allowed to settle for 12 h before introducing recombinant myostatin (R&D Systems). The cells were grown for 24 h before addition of 0.1 volume of AlamarBlue reagent and incubation at 37°C for 20 min before photometric analysis. The cells were then washed and cultured in fresh medium containing myostatin. Cell proliferation was monitored every 24 h for 4 days after initial introduction of myostatin. Cell number was determined by comparison of absorbance against a standard curve. All experiments were performed in triplicate.

RT-qPCR. Real-Time qPCR was performed according the SYBR Green® protocol (Applied Biosystems) on the Eco Real-Time PCR System (Illumina) with a HotStart Taq polymerase. For primer sequences see Online Supplementary Material. Fold changes were calculated according to the efficiency corrected $-\Delta\Delta C_t$ method. The use of normal and of DMD muscle from patients was covered by the approval of the ethical review board of the Charité (#216/2001). All patients or their legal guardians provided written informed consent according to the Declaration of Helsinki.

In vivo MRS investigation of muscle function and oxidative metabolism. Mice were anesthetized with 4% isoflurane in 100% air at a flow of 3 l/min and were placed into a home-built cradle specifically designed for the strictly noninvasive MRS investigation of muscle function and energetics[30]. Throughout the experiment, anesthesia was maintained using a facemask continuously supplying 1.75% isoflurane in 33% O_2 (0.2 l/min) and 66% N_2O (0.4 l/min). Animal body temperature was controlled by a rectal probe and maintained at physiological

values by a feedback loop that regulated an electrical heating blanket. MR spectra were recorded in the 4.7 T horizontal magnet of a 47/30 Biospec Avance MR system (Bruker, Karlsruhe, Germany) equipped with a Bruker 120-mm BGA12SL (200 mT/m) gradient insert. Calf muscle were electro-stimulated transcutaneously to produce maximal repeated isometric contractions at a frequency of 1.7 Hz. Mechanical performance was measured using a foot pedal coupled to a force transducer. Concentrations of phosphorylated compounds and intracellular pH of the calf muscle were continuously measured with an elliptic (8 x 12 mm^2) ^{31}P-MRS surface coil during 6 min of rest, 6 min of electro-stimulation and 16 min of recovery. MRS data were processed using a custom-written analysis program developed on the IDL software (Research System, Boulder, CO, USA). In order to determine the time constant of post-exercise phosphocreatine re-synthesis (τPCr, an *in vivo* index of oxidative mitochondrial capacity), the time course of phosphocreatine concentrations during the post-stimulation period was fitted to a mono-exponential function with a least mean-squared algorithm (**Fig. 5d**): $\tau PCr = -t/\ln(PCr_t/\Delta PCr)$, where ΔPCr is the extent of PCr depletion measured at the start of recovery period.

Statistical analysis. Data were analyzed and significance levels calculated using the non-parametric Wilcoxon-Mann-Whitney U-Test, as stated in the legends and detailed in the On-line Supplementary Material. Values are presented as means ± SEM (Standard Error of the Mean). Significance levels were set at $p<0.05$.

ACKNOWLEDGMENTS

We would like to acknowledge Acceleron Pharma for the gift of sActRIIB-Fc. This work was supported by the Association Française contre les Myopathies towards H.A., A.F., A.V., L.A., L.G., and E.M., Association Monegasque contre les Myopathies and the Parents Project France towards H.A. and C.H., Aktion Benni & Co towards H.A., the Deutsche Forschungsgemeinschaft and the Université Franco-Allemand towards K.R., H.A. and M.S. (as part of the MyoGrad International Graduate School for Myology DRK 1631/1 and CDFA-06-11), and NeuroCure (Exc 257) to M.S. The authors do not declare any conflict of interest.

AUTHORS' CONTRIBUTIONS

K.R., E.M., C.H., O.A., K.P., S.L., K.J., B.G., F.P.-R., L.A., A.V., D.F., S.B., A.F., M.S., H.A. performed the experiments; M.S. contributed patient material; O.R. contributed new reagents; K.R., E.M., D.F., S.B., B.G., D.B. A.F., R.V.C., M.S., H.A. analyzed the data; M.S. did the statistical analysis; K.R., E.M., B.G., D.B., M.S., H.A. wrote the manuscript, K.P. revised the article critically for important intellectual content. All authors read the final version of the manuscript and gave final approval of the manuscript to be published.

REFERENCES

1. McPherron, AC, Lawler, AM and Lee, SJ (1997) Regulation of skeletal muscle mass in mice by a new TGF-beta superfamily member. *Nature* **387**:83-90.

2. Lee, SJand McPherron, AC (2001) Regulation of myostatin activity and muscle growth. *Proc Natl Acad Sci U S A* **98**:9306-9311.

3. Schuelke, M, Wagner, KR, Stolz, LE, Hubner, C, Riebel, T, Komen, W *et al.* (2004) Myostatin mutation associated with gross muscle hypertrophy in a child. *N Engl J Med* **350**:2682-2688.

4. Amthor, H, Macharia, R, Navarrete, R, Schuelke, M, Brown, SC, Otto, A *et al.* (2007) Lack of myostatin results in excessive muscle growth but impaired force generation. *Proc Natl Acad Sci U S A* **104**:1835-1840.

5. Matsakas, A, Mouisel, E, Amthor, H and Patel, K (2010) Myostatin knockout mice increase oxidative muscle phenotype as an adaptive response to exercise. *J Muscle Res Cell Motil* **31**:111-125.

6. Qaisar, R, Renaud, G, Morine, K, Barton, ER, Sweeney, HL and Larsson, L (2012) Is functional hypertrophy and specific force coupled with the addition of myonuclei at the single muscle fiber level? *FASEB J* **26**:1077-1085.

7. Baligand, C, Gilson, H, Menard, JC, Schakman, O, Wary, C, Thissen, JP *et al.* (2010) Functional assessment of skeletal muscle in intact mice lacking myostatin by concurrent NMR imaging and spectroscopy. *Gene Ther* **17**:328-337.

8. Savage, KJand McPherron, AC (2010) Endurance exercise training in myostatin null mice. *Muscle Nerve* **42**:355-362.

9. Akpan, I, Goncalves, MD, Dhir, R, Yin, X, Pistilli, EE, Bogdanovich, S *et al.* (2009) The effects of a soluble activin type IIB receptor on obesity and insulin sensitivity. *Int J Obes (Lond)* **33**:1265-1273.

10. Cadena, SM, Tomkinson, KN, Monnell, TE, Spaits, MS, Kumar, R, Underwood, KW *et al.* (2010) Administration of a soluble activin type IIB receptor promotes skeletal muscle growth independent of fiber type. *J Appl Physiol* **109**:635-642.

11. Morine, KJ, Bish, LT, Selsby, JT, Gazzara, JA, Pendrak, K, Sleeper, MM *et al.* (2010) Activin IIB receptor blockade attenuates dystrophic pathology in a mouse model of Duchenne muscular dystrophy. *Muscle Nerve* **42**:722-730.

12. Pistilli, EE, Bogdanovich, S, Goncalves, MD, Ahima, RS, Lachey, J, Seehra, J *et al.* (2011) Targeting the activin type IIB receptor to improve muscle mass and function in the mdx mouse model of Duchenne muscular dystrophy. *Am J Pathol* **178**:1287-1297.

13. Rahimov, F, King, OD, Warsing, LC, Powell, RE, Emerson, CP, Jr., Kunkel, LM *et al.* (2011) Gene expression profiling of skeletal muscles treated with a soluble activin type IIB receptor. *Physiol Genomics* **43**:398-407.

14. Chiu, CS, Peekhaus, N, Weber, H, Adamski, S, Murray, EM, Zhang, HZ *et al.* (2013) Increased muscle force production and bone mineral density in ActRIIB-Fc-treated mature rodents. *J Gerontol A Biol Sci Med Sci* **68**:1181-1192.

15. Jongpiputvanich, S, Sueblinvong, T and Norapucsunton, T (2005) Mitochondrial respiratory chain dysfunction in various neuromuscular diseases. *J Clin Neurosci* **12**:426-428.

16. Kuznetsov, AV, Winkler, K, Wiedemann, FR, von, BP, Dietzmann, K and Kunz, WS (1998) Impaired mitochondrial oxidative phosphorylation in skeletal muscle of the dystrophin-deficient mdx mouse. *Mol Cell Biochem* **183**:87-96.

17. Millay, DP, Sargent, MA, Osinska, H, Baines, CP, Barton, ER, Vuagniaux, G *et al.* (2008) Genetic and pharmacologic inhibition of mitochondrial-dependent necrosis attenuates muscular dystrophy. *Nat Med* **14**:442-447.

18. Girgenrath, S, Song, K and Whittemore, LA (2005) Loss of myostatin expression alters fiber-type distribution and expression of myosin heavy chain isoforms in slow- and fast-type skeletal muscle. *Muscle Nerve* **31**:34-40.

19. Matsakas, A, Macharia, R, Otto, A, Elashry, MI, Mouisel, E, Romanello, V *et al.* (2012) Exercise training attenuates the hypermuscular phenotype and restores skeletal muscle function in the myostatin null mouse. *Exp Physiol* **97**:125-140.

20. Lee, SJ, Reed, LA, Davies, MV, Girgenrath, S, Goad, ME, Tomkinson, KN *et al.* (2005) Regulation of muscle growth by multiple ligands signaling through activin type II receptors. *Proc Natl Acad Sci U S A* **102**:18117-18122.

21. Billat, VL, Mouisel, E, Roblot, N and Melki, J (2005) Inter- and intrastrain variation in mouse critical running speed. *J Appl Physiol* **98**:1258-1263.

22. Han, JJ, Carter, GT, Ra, JJ, Abresch, RT, Chamberlain, JS and Robinson, LR (2006) Electromyographic studies in mdx and wild-type C57 mice. *Muscle Nerve* **33**:208-214.

23. Hayot, M, Rodriguez, J, Vernus, B, Carnac, G, Jean, E, Allen, D *et al.* (2011) Myostatin up-regulation is associated with the skeletal muscle response to hypoxic stimuli. *Mol Cell Endocrinol* **332**:38-47.

24. Zhao, G, Jeoung, NH, Burgess, SC, Rosaaen-Stowe, KA, Inagaki, T, Latif, S *et al.* (2008) Overexpression of pyruvate dehydrogenase kinase 4 in heart perturbs metabolism and exacerbates calcineurin-induced cardiomyopathy. *Am J Physiol Heart Circ Physiol* **294**:H936-H943.

25. Brenman, JE, Chao, DS, Xia, H, Aldape, K and Bredt, DS (1995) Nitric oxide synthase complexed with dystrophin and absent from skeletal muscle sarcolemma in Duchenne muscular dystrophy. *Cell* **82**:743-752.

26. Chang, WJ, Iannaccone, ST, Lau, KS, Masters, BS, McCabe, TJ, McMillan, K *et al.* (1996) Neuronal nitric oxide synthase and dystrophin-deficient muscular dystrophy. *Proc Natl Acad Sci U S A* **93**:9142-9147.

27. Heydemann, A and McNally, E (2009) NO more muscle fatigue. *J Clin Invest* **119**:448-450.

28. Kobayashi, YM, Rader, EP, Crawford, RW, Iyengar, NK, Thedens, DR, Faulkner, JA *et al.* (2008) Sarcolemma-localized nNOS is required to maintain activity after mild exercise. *Nature* **456**:511-515.

29. Percival, JM, Siegel, MP, Knowels, G and Marcinek, DJ (2013) Defects in mitochondrial localization and ATP synthesis in the mdx mouse model of Duchenne muscular dystrophy are not alleviated by PDE5 inhibition. *Hum Mol Genet* **22**:153-167.

30. Giannesini, B, Vilmen, C, Le, FY, Dalmasso, C, Cozzone, PJ and Bendahan, D (2010) A strictly noninvasive MR setup dedicated to longitudinal studies of mechanical performance, bioenergetics, anatomy, and muscle recruitment in contracting mouse skeletal muscle. *Magn Reson Med* **64**:262-270.

31. Guzun, R, Gonzalez-Granillo, M, Karu-Varikmaa, M, Grichine, A, Usson, Y, Kaambre, T *et al.* (2012) Regulation of respiration in muscle cells in vivo by VDAC through interaction with the cytoskeleton and MtCK within Mitochondrial Interactosome. *Biochim Biophys Acta* **1818**:1545-1554.

32. Braun, U, Paju, K, Eimre, M, Seppet, E, Orlova, E, Kadaja, L *et al.* (2001) Lack of dystrophin is associated with altered integration of the mitochondria and ATPases in slow-twitch muscle cells of MDX mice. *Biochim Biophys Acta* **1505**:258-270.

33. Massa, R, Marliera, LN, Martorana, A, Cicconi, S, Pierucci, D, Giacomini, P *et al.* (2000) Intracellular localization and isoform expression of the voltage-dependent anion channel (VDAC) in normal and dystrophic skeletal muscle. *J Muscle Res Cell Motil* **21**:433-442.

34. Lewis, C, Jockusch, H and Ohlendieck, K (2010) Proteomic Profiling of the Dystrophin-Deficient MDX Heart Reveals Drastically Altered Levels of Key Metabolic and Contractile Proteins. *J Biomed Biotechnol* **2010**:648501.

35. Janssen, AJ, Schuelke, M, Smeitink, JA, Trijbels, FJ, Sengers, RC, Lucke, B *et al.* (2008) Muscle 3243A>G mutation load and capacity of the mitochondrial energy-generating system. *Ann Neurol* **63**:473-481.

36. Mosher, DS, Quignon, P, Bustamante, CD, Sutter, NB, Mellersh, CS, Parker, HG *et al.* (2007) A mutation in the myostatin gene increases muscle mass and enhances racing performance in heterozygote dogs. *PLoS Genet* **3**:e79.

37. Grobet, L, Martin, LJ, Poncelet, D, Pirottin, D, Brouwers, B, Riquet, J *et al.* (1997) A deletion in the bovine myostatin gene causes the double-muscled phenotype in cattle. *Nat Genet* **17**:71-74.

38. McPherron, ACand Lee, SJ (1997) Double muscling in cattle due to mutations in the myostatin gene. *Proc Natl Acad Sci U S A* **94**:12457-12461.

39. Holmes, JH, Robinson, DW and Ashmore, CR (1972) Blood lactic acid and behaviour in cattle with hereditary muscular hypertrophy. *J Anim Sci* **35**:1011-1013.

40. Holmes, JH, Ashmore, CR and Robinson, DW (1973) Effects of stress on cattle with hereditary muscular hypertrophy. *J Anim Sci* **36**:684-694.

41. Personius, KE, Jayaram, A, Krull, D, Brown, R, Xu, T, Han, B *et al.* (2010) Grip force, EDL contractile properties, and voluntary wheel running after postdevelopmental myostatin depletion in mice. *J Appl Physiol* **109**:886-894.

42. Sander, M, Chavoshan, B, Harris, SA, Iannaccone, ST, Stull, JT, Thomas, GD *et al.* (2000) Functional muscle ischemia in neuronal nitric oxide synthase-deficient skeletal muscle of children with Duchenne muscular dystrophy. *Proc Natl Acad Sci U S A* **97**:13818-13823.

43. George, CC, Bruemmer, K, Sesti, J, Stefanski, C, Curtis, H, Ucran, J *et al.* (2011) Soluble activin receptor type IIB increases forward pulling tension in the mdx mouse. *Muscle Nerve* **43**:694-699.

44. Lach-Trifilieff, E, Minetti, GC, Sheppard, K, Ibebunjo, C, Feige, JN, Hartmann, S *et al.* (2014) An antibody blocking activin type II receptors induces strong skeletal muscle hypertrophy and protects from atrophy. *Mol Cell Biol* **34**:606-618.

45. Goemans, N, Klingels, K, van den, HM, Boons, S, Verstraete, L, Peeters, C *et al.* (2013) Six-minute walk test: reference values and prediction equation in healthy boys aged 5 to 12 years. *PLoS One* **8**:e84120.

46. Schuler, M, Ali, F, Chambon, C, Duteil, D, Bornert, JM, Tardivel, A *et al.* (2006) PGC1alpha expression is controlled in skeletal muscles by PPARbeta, whose ablation results in fiber-type switching, obesity, and type 2 diabetes. *Cell Metab* **4**:407-414.

47. Robergs, RA, Ghiasvand, F and Parker, D (2004) Biochemistry of exercise-induced metabolic acidosis. *Am J Physiol Regul Integr Comp Physiol* **287**:R502-R516.

48. Lebrasseur, NK, Schelhorn, TM, Bernardo, BL, Cosgrove, PG, Loria, PM and Brown, TA (2009) Myostatin inhibition enhances the effects of exercise on performance and metabolic outcomes in aged mice. *J Gerontol A Biol Sci Med Sci* **64**:940-948.

49. Morrison, BM, Lachey, JL, Warsing, LC, Ting, BL, Pullen, AE, Underwood, KW *et al.* (2009) A soluble activin type IIB receptor improves function in a mouse model of amyotrophic lateral sclerosis. *Exp Neurol* **217**:258-268.

50. Rajab, A, Straub, V, McCann, LJ, Seelow, D, Varon, R, Barresi, R *et al.* (2010) Fatal cardiac arrhythmia and long-QT syndrome in a new form of congenital generalized lipodystrophy with muscle rippling (CGL4) due to PTRF-CAVIN mutations. *PLoS Genet* **6**:e1000874.

FIGURE LEGENDS

Figure 1: Treatment of adult wild-type mice with sActRIIB-Fc. All tests were done after a 4 months treatment of the wild-type mice with either sActRIIB-Fc or PBS (controls). **(a)** Absolute maximal force (n=10 for each condition), and **(b)** specific maximal force of *EDL* and *soleus* muscles (n=10 for each condition). **(c)** Force recordings during the fatigue protocol over 180 s, and **(d)** Fatigue resistance of *EDL* (n=9 for PBS treated mice and n=8 for sActRIIB-Fc treated mice) and *soleus* muscles (n=10 for PBS treated mice and n=9 for sActRIIB-Fc treated mice). **(e)** Running distances during incremental speed running until exhaustion (n=5 for each condition). **(f)** Serum lactate levels at rest and 5 min after incremental speed running until exhaustion (n=5 for each condition). **(g)** A plot depicting the relationship between travel distance until exhaustion during incremental speed running and serum lactate, which was measured 5 min after exhaustion, for individual mice (n=5 for each condition). **(h)** Critical Speed before and after 1, 2 and 4 months of treatment with sActRIIB-Fc in comparison to PBS-treated control mice (n=5 for each condition). **(i)** A plot depicts the proportional relationship between distance run (y-axis) and time to exhaustion (x-axis) at different velocities. The slope of the regression line indicates the Critical Speed. Values are shown as means ± SEM. p-Values were calculated using the nonparametric U-Test.

Figure 2: Treatment of adult *mdx* mice with sActRIIB-Fc. All tests were performed after a 4 months treatment of the *mdx* mice with either sActRIIB-Fc or PBS (controls). **(a)** Absolute maximal force (n=9 for each condition for *EDL* muscles and n=10 for each condition for *soleus* muscles), and **(b)** specific maximal force of *EDL* (n=9 for each condition) and *soleus* muscles (n=10 for each condition). **(c)** Force recordings during the fatigue protocol over 180 s of *EDL* and *soleus* muscles, and **(d)** fatigue resistance for *EDL* (n=8 for each condition) and *soleus* (n=10 for PBS treated mice and n=8 for sActRIIB-Fc treated mice). **(e)** Running distance during incremental speed running until exhaustion (n=5 for each condition). **(f)** Serum lactate levels at rest and 5 min after incremental speed running until exhaustion (n=5 for each condition). **(g)** A plot depicts the relationship between travel distance until exhaustion during incremental speed running and serum lactate, which was measured 5 min after exhaustion, for individual mice (n=5 for each condition). **(h)** Critical Speed before and after 1, 2 and 4 months of treatment with sActRIIB-Fc in comparison to PBS (n=5 for each condition). **(i)** A plot depicts the proportional relationship between distance run (y-axis) and time to exhaustion (x-axis) at different velocities. The slope of the regression line indicates the Critical Speed.

Values are shown as means ± SEM. p-Values were calculated using the nonparametric U-Test.

Figure 3: The effect of myostatin/ActRIIB signaling on vascularization. All investigations were done after a 4 months treatment of wild-type and *mdx* mice with either sActRIIB-Fc or PBS (controls). **(a-d)** Capillarization of wild-type *soleus* (n=430 fibers from PBS treated muscles (n=3) and n=300 fibers from sActRIIB-Fc treated muscles (n=3)) and *mdx soleus* muscle (n=605 fibers from PBS treated muscles (n=3) and n=836 fibers from sActRIIB-Fc treated muscles (n=4)). Histograms in **(a)** and **(c)** depict the distribution of capillaries per muscle fiber (in [%]), whereas diagrams in **(b)** and **(d)** depict the capillary domain, the fiber area per capillary (in [μm^2]). Values are depicted as means ± SEM. **(e)** *Vegf-A* relative mRNA-copy numbers as expressed per 10^6 x 18S rRNA copies in wild-type *TA* muscle (n=5 for each condition). **(f)** *Vegf-A* relative mRNA-copy numbers in C_2C_{12} myotubes following 24 h treatment with sActRIIB-Fc in comparison to control cultures (n=3 for each condition). **(g)** Relative mRNA-copy numbers of *MSTN* and myostatin receptors *ActRIIA/B* and *ALK4/5* in cultures of human umbilical vein endothelial cells (HUVEC) in comparison to muscle samples from a healthy control and a patient with Duchenne muscular dystrophy. Values are shown as means ± SEM. p-Values were calculated using the nonparametric U-Test.

Figure 4: Effect of myostatin/ActRIIB signaling on muscle metabolic phenotype. All investigations were done after a 4 months treatment of wild-type (n=5 for each condition) and *mdx* mice (n=5 for each condition) with either sActRIIB-Fc or PBS (controls). **(a)** Western blots (left side) depict bands for Pgc1α referenced to Desmin. The bar chart (right side) depicts the quotients of Pgc1α/Desmin band densities. **(b)** *Pgc1α* and **(c)** *Pparβ* relative copy numbers in the *TA* muscle from wild-type and *mdx* mice as expressed per 10^6 x 18S rRNA copies. **(d)** Enolase enzymatic activity in wildtype *EDL* (n=5 for each condition) and wildtype *soleus* muscles (n=5 for each condition). **(e-f)** Relative mRNA-copy numbers of genes involved in the regulation of the oxidative metabolism in *TA* muscle from wild-type and *mdx* mice and **(g)** from C_2C_{12} myotubes following 24 h treatment with sActRIIB-Fc in comparison to control cultures (n=3 for each condition). Values are shown as means ± SEM. p-Values were calculated using the nonparametric U-Test.

Figure 5: *In vivo* investigation of muscle function and oxidative metabolism in *mdx* calf muscles by non-invasive ^{31}P-MRS. Investigations were done in *mdx* mice that were treated either with sActRIIB-Fc (n=5) or with PBS (controls; n=4). (**a**) The extent of force reduction was measured at the end of the 6 min period of electro-stimulation and is represented as per-

cent of the starting value. (**b**) The drop of intracellular pH and (**c**) phosphocreatine (PCr) concentration was determined at the end of the 6 min *in vivo* electro-stimulation period. (**d**) For each animal, the post-stimulation time course of PCr was fitted to a mono-exponential function with a least mean-squared algorithm in order to calculate the PCr recovery time constant (τPCr): $\tau PCr = -t/\ln(PCr_t/\Delta PCr)$. (**e**) τPCr was significantly larger in sActRIIB-Fc treated *mdx* mice (200 ± 39 s *versus* 78 ± 20 s in the control group). Values are shown as means ± SEM. p-Values were calculated using the nonparametric U-Test.

Figure 1

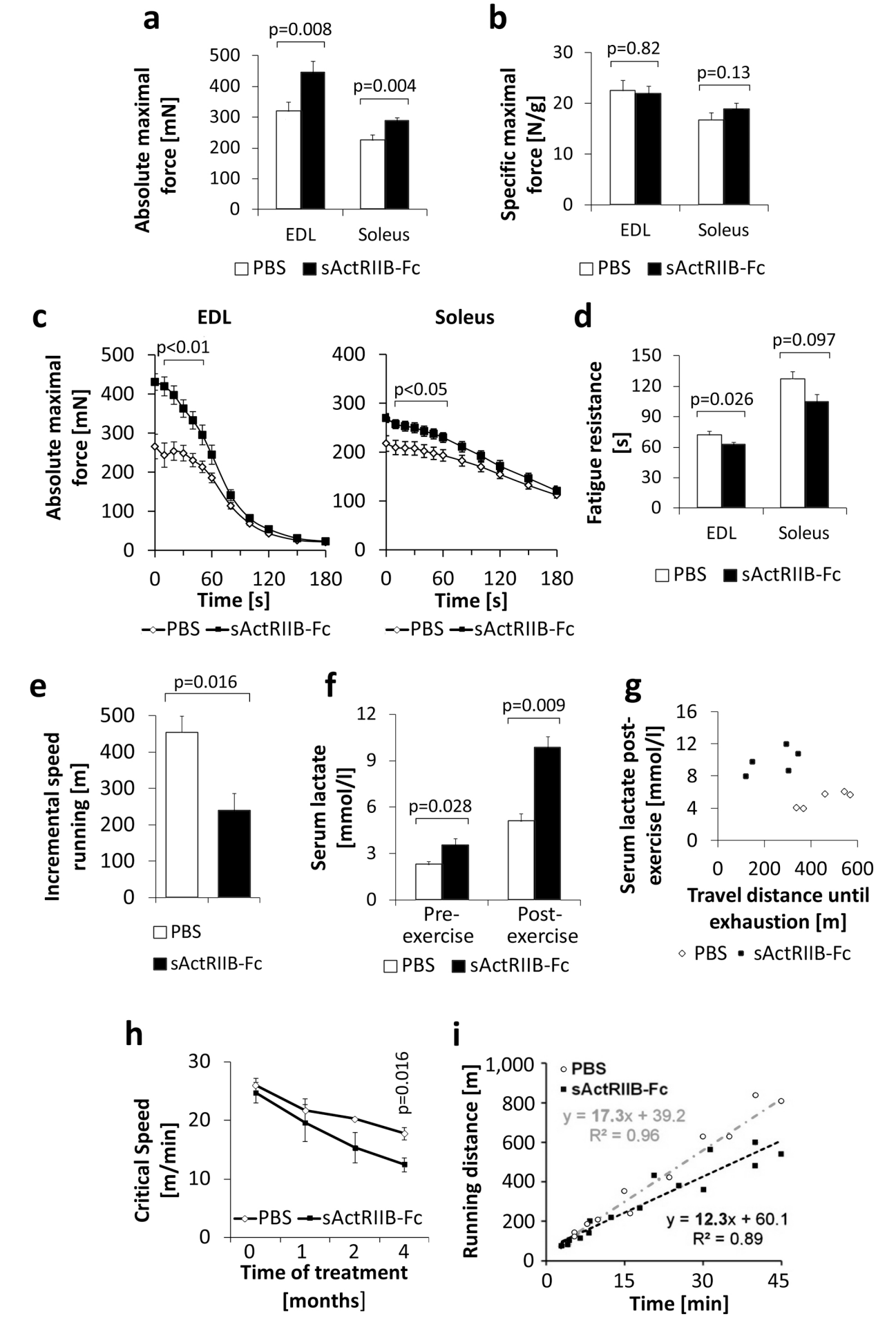
a
p=0.008
p=0.004
Absolute maximal force [mN]
500
400
300
200
100
0
EDL
Soleus
PBS
sActRIIB-Fc
b
p=0.82
p=0.13
Specific maximal force [N/g]
30
20
10
0
EDL
Soleus
PBS
sActRIIB-Fc
c
EDL
Soleus
p<0.01
p<0.05
Absolute maximal force [mN]
Time [s]
0
60
120
180
PBS
sActRIIB-Fc
d
p=0.026
p=0.097
Fatigue resistance [s]
150
120
90
60
30
0
EDL
Soleus
PBS
sActRIIB-Fc
e
p=0.016
Incremental speed running [m]
500
400
300
200
100
0
PBS
sActRIIB-Fc
f
p=0.028
p=0.009
Serum lactate [mmol/l]
12
9
6
3
0
Pre-exercise
Post-exercise
PBS
sActRIIB-Fc
g
Serum lactate post-exercise [mmol/l]
16
12
8
4
0
0
200
400
600
Travel distance until exhaustion [m]
PBS
sActRIIB-Fc
h
p=0.016
Critical Speed [m/min]
30
20
10
0
PBS
sActRIIB-Fc
0
1
2
4
Time of treatment [months]
i
PBS
sActRIIB-Fc
y = 17.3x + 39.2
R² = 0.96
y = 12.3x + 60.1
R² = 0.89
Running distance [m]
1,000
800
600
400
200
0
0
15
30
45
Time [min]

Figure 2

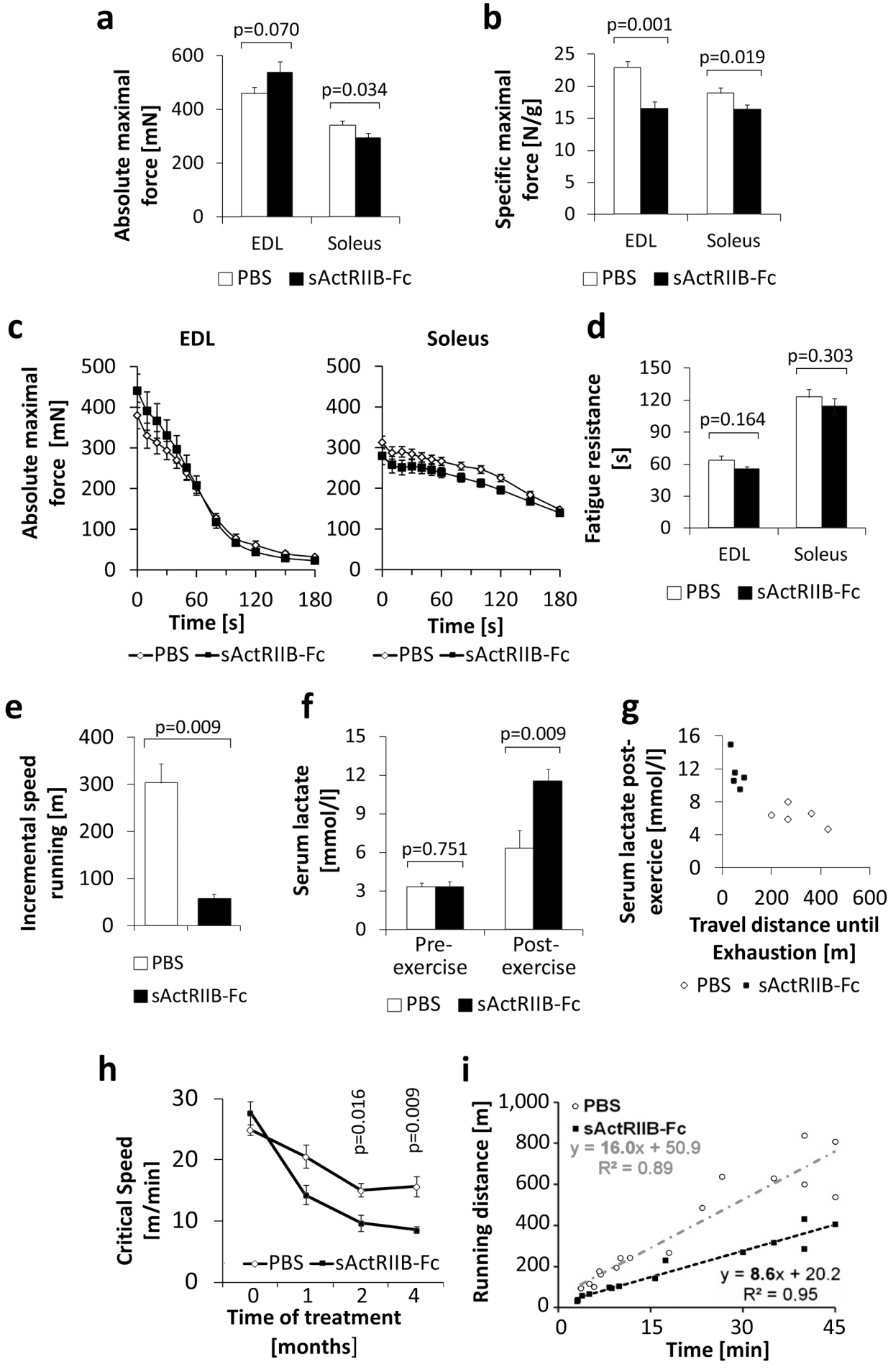
a
p=0.070
p=0.034
Absolute maximal force [mN]
600
400
200
0
EDL
Soleus
PBS
sActRIIB-Fc
b
p=0.001
p=0.019
Specific maximal force [N/g]
25
20
15
10
5
0
EDL
Soleus
PBS
sActRIIB-Fc
c
EDL
Soleus
Absolute maximal force [mN]
500
400
300
200
100
0
0
60
120
180
Time [s]
PBS
sActRIIB-Fc
d
p=0.164
p=0.303
Fatigue resistance [s]
150
120
90
60
30
0
EDL
Soleus
PBS
sActRIIB-Fc
e
p=0.009
Incremental speed running [m]
400
300
200
100
0
PBS
sActRIIB-Fc
f
p=0.751
p=0.009
Serum lactate [mmol/l]
15
12
9
6
3
0
Pre-exercise
Post-exercise
PBS
sActRIIB-Fc
g
Serum lactate post-exercice [mmol/l]
16
12
8
4
0
0
200
400
600
Travel distance until Exhaustion [m]
PBS
sActRIIB-Fc
h
p=0.016
p=0.009
Critical Speed [m/min]
30
20
10
0
PBS
sActRIIB-Fc
0
1
2
4
Time of treatment [months]
i
PBS
sActRIIB-Fc
y = 16.0x + 50.9
R² = 0.89
y = 8.6x + 20.2
R² = 0.95
Running distance [m]
1,000
800
600
400
200
0
0
15
30
45
Time [min]

Figure 3

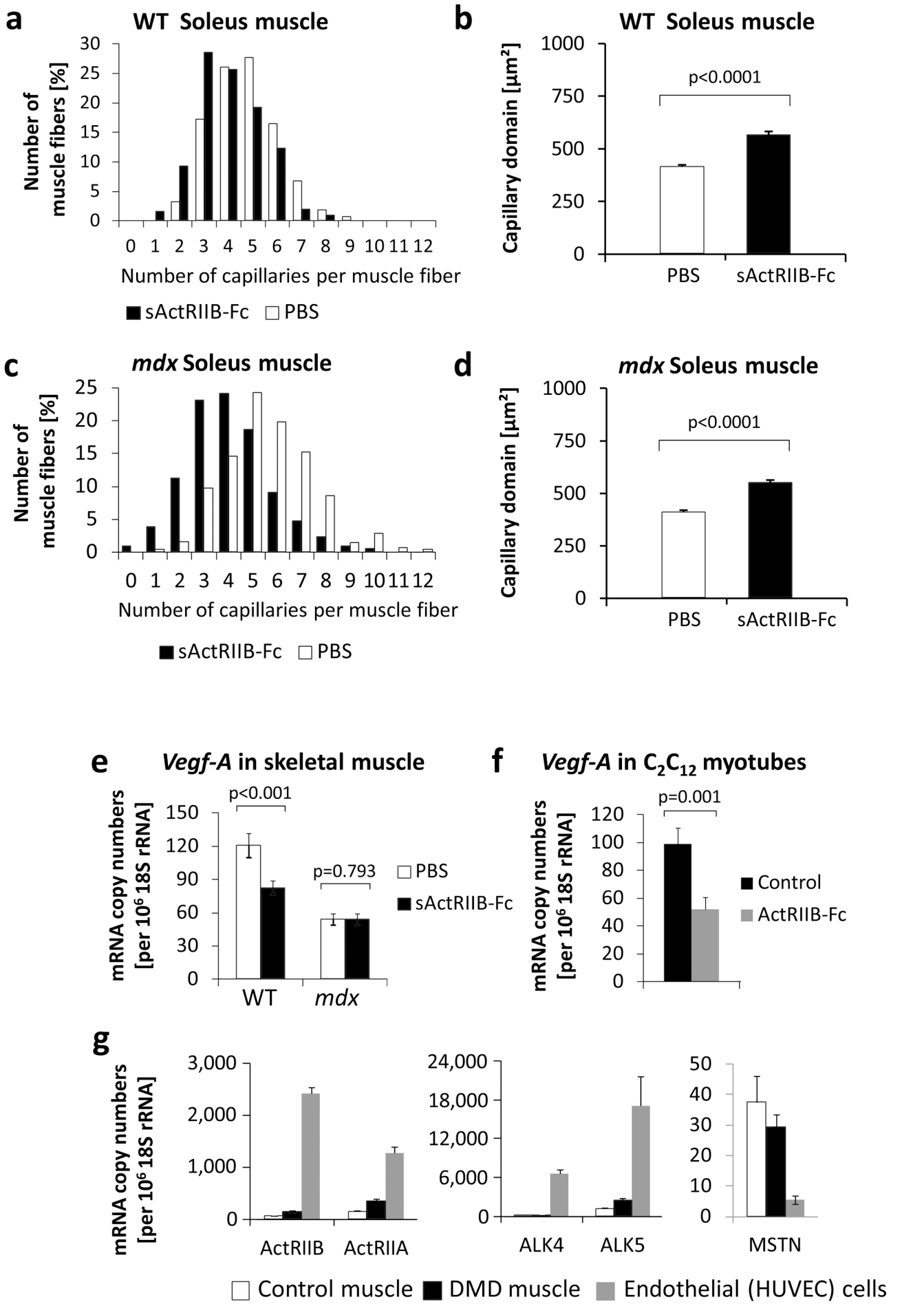
a
WT Soleus muscle
Number of muscle fibers [%]
Number of capillaries per muscle fiber
sActRIIB-Fc
PBS
b
WT Soleus muscle
Capillary domain [µm²]
p<0.0001
PBS
sActRIIB-Fc
c
mdx Soleus muscle
Number of muscle fibers [%]
Number of capillaries per muscle fiber
sActRIIB-Fc
PBS
d
mdx Soleus muscle
Capillary domain [µm²]
p<0.0001
PBS
sActRIIB-Fc
e
Vegf-A in skeletal muscle
mRNA copy numbers [per 10⁶ 18S rRNA]
p<0.001
p=0.793
PBS
sActRIIB-Fc
WT
mdx
f
Vegf-A in C2C12 myotubes
mRNA copy numbers [per 10⁶ 18S rRNA]
p=0.001
Control
ActRIIB-Fc
g
mRNA copy numbers [per 10⁶ 18S rRNA]
ActRIIB
ActRIIA
ALK4
ALK5
MSTN
Control muscle
DMD muscle
Endothelial (HUVEC) cells

Figure 4

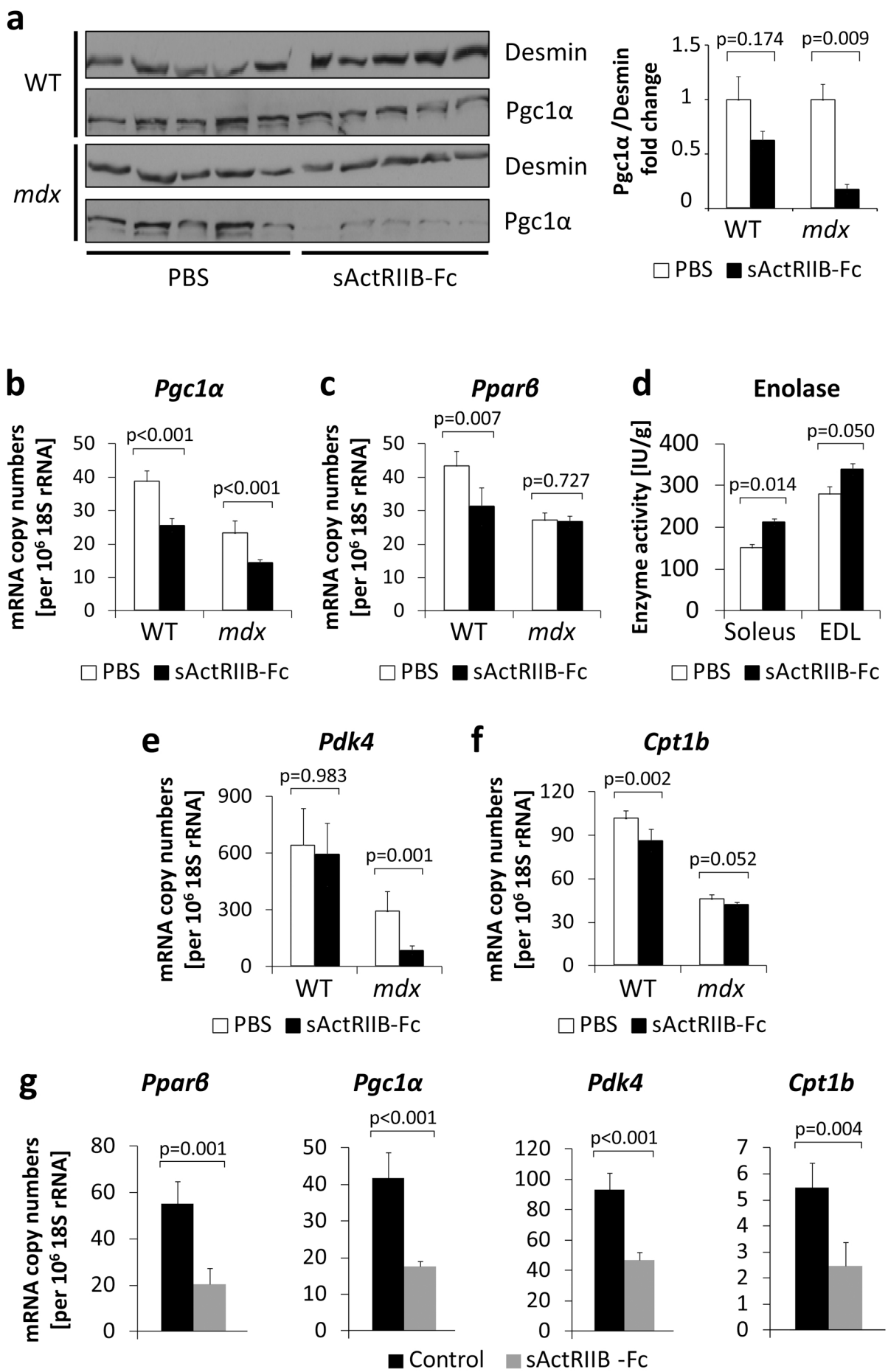
a
WT
mdx
Desmin
Pgc1α
Desmin
Pgc1α
PBS
sActRIIB-Fc
Pgc1α /Desmin fold change
p=0.174
p=0.009
WT
mdx
PBS
sActRIIB-Fc
b
Pgc1α
mRNA copy numbers [per 10⁶ 18S rRNA]
p<0.001
p<0.001
WT
mdx
PBS
sActRIIB-Fc
c
Pparβ
p=0.007
p=0.727
d
Enolase
Enzyme activity [IU/g]
p=0.014
p=0.050
Soleus
EDL
e
Pdk4
p=0.983
p=0.001
f
Cpt1b
p=0.002
p=0.052
g
Pparβ
Pgc1α
Pdk4
Cpt1b
p=0.001
p<0.001
p<0.001
p=0.004
Control
sActRIIB -Fc

Figure 5

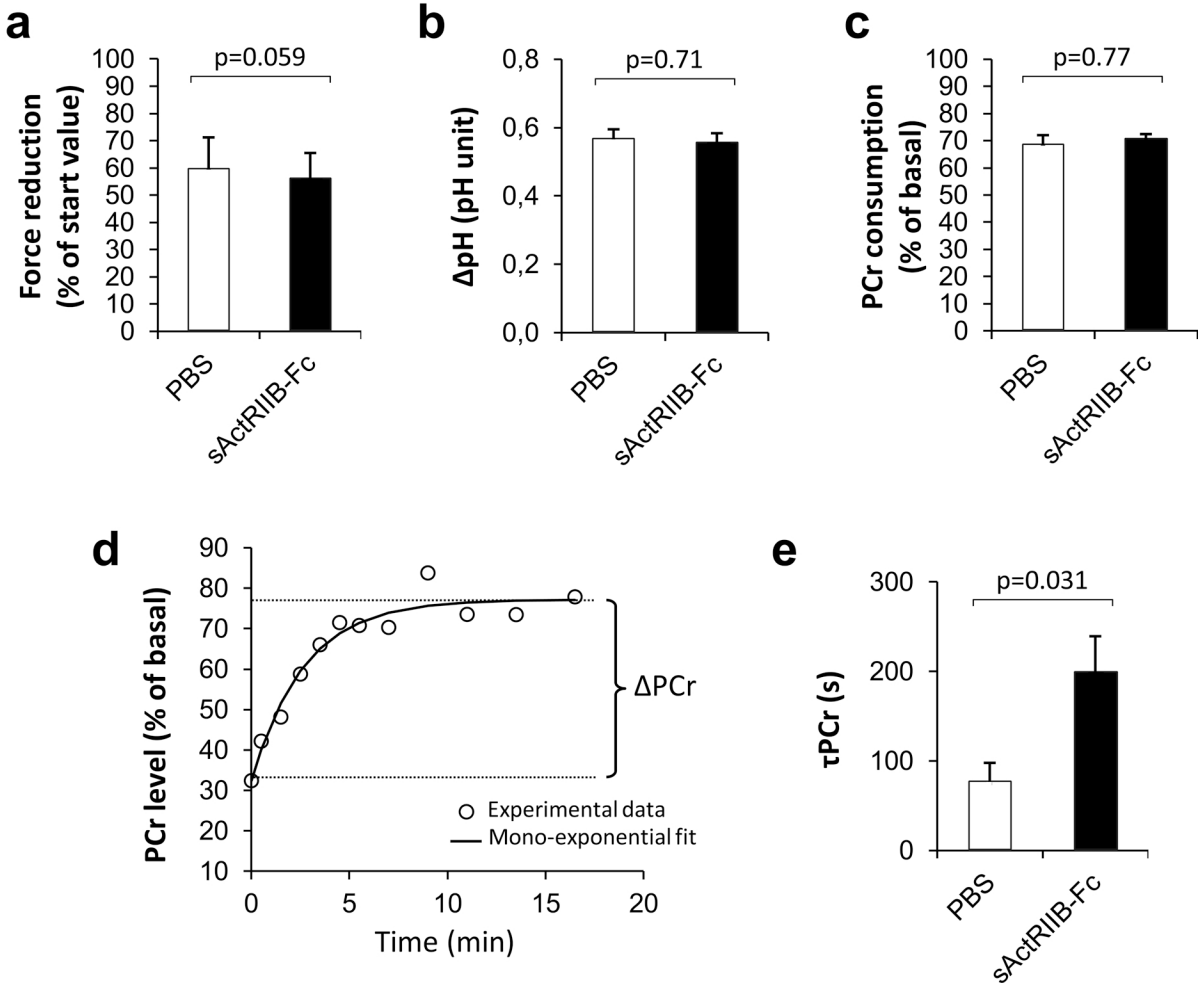
a
Force reduction (% of start value)
p=0.059
PBS
sActRIIB-Fc
b
ΔpH (pH unit)
p=0.71
PBS
sActRIIB-Fc
c
PCr consumption (% of basal)
p=0.77
PBS
sActRIIB-Fc
d
PCr level (% of basal)
ΔPCr
Experimental data
Mono-exponential fit
Time (min)
e
τPCr (s)
p=0.031
PBS
sActRIIB-Fc